

# The Silicon Vertex Detector of the Belle II Experiment

Y. Uematsu<sup>q</sup>, K. Adamczyk<sup>t</sup>, L. Aggarwal<sup>i</sup>, H. Aihara<sup>q</sup>, T. Aziz<sup>j</sup>, S. Bacher<sup>t</sup>, S. Bahinipati<sup>f</sup>, G. Batignani<sup>k,l</sup>, J. Baudot<sup>e</sup>, P. K. Behera<sup>g</sup>, S. Bettarini<sup>k,l</sup>, T. Bilka<sup>c</sup>, A. Bozek<sup>t</sup>, F. Buchsteiner<sup>b</sup>, G. Casarosa<sup>k,l</sup>, L. Corona<sup>k,l</sup>, T. Czank<sup>p</sup>, S. B. Das<sup>h</sup>, G. Dujany<sup>e</sup>, C. Finck<sup>e</sup>, F. Forti<sup>k,l</sup>, M. Friedl<sup>b</sup>, A. Gabrielli<sup>m,n</sup>, E. Ganiev<sup>m,n</sup>, B. Gobbo<sup>n</sup>, S. Halder<sup>j</sup>, K. Hara<sup>r,o</sup>, S. Hazra<sup>j</sup>, T. Higuchi<sup>p</sup>, C. Irmeler<sup>b</sup>, A. Ishikawa<sup>r,o</sup>, H. B. Jeon<sup>s</sup>, Y. Jin<sup>m,n</sup>, C. Joo<sup>p</sup>, M. Kaleta<sup>t</sup>, A. B. Kaliyar<sup>j</sup>, J. Kandra<sup>c</sup>, K. H. Kang<sup>s</sup>, P. Kapusta<sup>t</sup>, P. Kodyš<sup>c</sup>, T. Kohriki<sup>f</sup>, M. Kumar<sup>h</sup>, R. Kumar<sup>i</sup>, C. La Licata<sup>p</sup>, K. Lalwani<sup>h</sup>, R. Leboucher<sup>d</sup>, S. C. Lee<sup>s</sup>, J. Libby<sup>g</sup>, L. Martel<sup>e</sup>, L. Massacesi<sup>k,l</sup>, S. N. Mayekar<sup>j</sup>, G. B. Mohanty<sup>j</sup>, T. Morii<sup>p</sup>, K. R. Nakamura<sup>r,o</sup>, Z. Natkaniec<sup>t</sup>, Y. Onuki<sup>q</sup>, W. Ostrowicz<sup>t</sup>, A. Paladino<sup>k,l</sup>, E. Paoloni<sup>k,l</sup>, H. Park<sup>s</sup>, L. Polat<sup>d</sup>, K. K. Rao<sup>j</sup>, I. Ripp-Baudot<sup>e</sup>, G. Rizzo<sup>k,l</sup>, D. Sahoo<sup>j</sup>, C. Schwanda<sup>b</sup>, J. Serrano<sup>d</sup>, J. Suzuki<sup>r</sup>, S. Tanaka<sup>r,o</sup>, H. Tanigawa<sup>q</sup>, R. Thalmeier<sup>b</sup>, R. Tiwari<sup>j</sup>, T. Tsuboyama<sup>r,o</sup>, O. Verbycka<sup>t</sup>, L. Vitale<sup>m,n</sup>, K. Wan<sup>q</sup>, Z. Wang<sup>q</sup>, J. Webb<sup>a</sup>, J. Wiechczynski<sup>l</sup>, H. Yin<sup>b</sup>, L. Zani<sup>d</sup>,

(Belle-II SVD Collaboration)

<sup>a</sup>*School of Physics, University of Melbourne, Melbourne, Victoria 3010, Australia*

<sup>b</sup>*Institute of High Energy Physics, Austrian Academy of Sciences, 1050 Vienna, Austria*

<sup>c</sup>*Faculty of Mathematics and Physics, Charles University, 121 16 Prague, Czech Republic*

<sup>d</sup>*Aix Marseille Université, CNRS/IN2P3, CPPM, 13288 Marseille, France*

<sup>e</sup>*IPHC, UMR 7178, Université de Strasbourg, CNRS, 67037 Strasbourg, France*

<sup>f</sup>*Indian Institute of Technology Bhubaneswar, Satya Nagar, India*

<sup>g</sup>*Indian Institute of Technology Madras, Chennai 600036, India*

<sup>h</sup>*Malaviya National Institute of Technology Jaipur, Jaipur 302017, India*

<sup>i</sup>*Punjab Agricultural University, Ludhiana 141004, India*

<sup>j</sup>*Tata Institute of Fundamental Research, Mumbai 400005, India*

<sup>k</sup>*Dipartimento di Fisica, Università di Pisa, I-56127 Pisa, Italy*

<sup>l</sup>*INFN Sezione di Pisa, I-56127 Pisa, Italy*

<sup>m</sup>*Dipartimento di Fisica, Università di Trieste, I-34127 Trieste, Italy*

<sup>n</sup>*INFN Sezione di Trieste, I-34127 Trieste, Italy*

<sup>o</sup>*The Graduate University for Advanced Studies (SOKENDAI), Hayama 240-0193, Japan*

<sup>p</sup>*Kavli Institute for the Physics and Mathematics of the Universe (WPI), University of Tokyo, Kashiwa 277-8583, Japan*

<sup>q</sup>*Department of Physics, University of Tokyo, Tokyo 113-0033, Japan*

<sup>r</sup>*High Energy Accelerator Research Organization (KEK), Tsukuba 305-0801, Japan*

<sup>s</sup>*Department of Physics, Kyungpook National University, Daegu 41566, Korea*

<sup>t</sup>*H. Niewodniczanski Institute of Nuclear Physics, Krakow 31-342, Poland*

---

## Abstract

The Silicon Vertex Detector (SVD) is a part of the vertex detector in the Belle II experiment at the SuperKEKB collider (KEK, Japan). Since the start of data taking in spring 2019, the SVD has been operating stably and reliably with a high signal-to-noise ratio and hit efficiency, achieving good spatial resolution and high track reconstruction efficiency. The hit occupancy, which mostly comes from the beam-related background, is currently about 0.5% in the innermost layer, causing no impact on the SVD performance. In anticipation of the operation at higher luminosity in the next years, two strategies to sustain the tracking performance in future high beam background conditions have been developed and tested on data. One is to reduce the number of signal waveform samples to decrease dead time, data size, and occupancy. The other is to utilize the good hit-time resolution to reject the beam background hits. We also measured the radiation effects on the sensor current, strip noise, and full depletion voltage caused during the first two and a half years of operation. The results show no detrimental effect on the SVD performance.

**Keywords:** Silicon strip detector, Vertex detector, Tracking detector, Belle II

---

## 1. Introduction

The Belle II experiment [1] aims to probe new physics beyond the Standard Model in high-luminosity  $e^+e^-$  collisions at the SuperKEKB collider (KEK, Japan) [2]. The main collision energy in the center-of-mass system is 10.58 GeV on the  $\Upsilon(4S)$  resonance, which enables various physics programs based on

the large samples of B mesons,  $\tau$  leptons, and D mesons. Also, the asymmetric energy of the 7 GeV electron beam and 4 GeV positron beam is adopted for time-dependent  $CP$  violation measurements. The target of SuperKEKB is to accumulate an integrated luminosity of 50  $\text{ab}^{-1}$  with peak luminosity of about  $6 \times 10^{35} \text{ cm}^{-2}\text{s}^{-1}$ . In June 2021, SuperKEKB recorded the world's highest instantaneous luminosity of  $3.1 \times 10^{34} \text{ cm}^{-2}\text{s}^{-1}$ . The data accumulated before July 2021 corresponds to an integrated luminosity of 213  $\text{fb}^{-1}$ .

---

Email address: uematsu@hep.phys.s.u-tokyo.ac.jp (Y. Uematsu)

16 The Vertex Detector (VXD) is the innermost detector in the 55  
 17 Belle II detector system. The VXD has six layers: the inner 56  
 18 two layers (layers 1 and 2) are the Pixel Detector (PXD), and 57  
 19 the outer four layers (layers 3 to 6) are the Silicon Vertex Detec- 58  
 20 tor (SVD). The schematic cross-sectional view of the VXD is 59  
 21 shown in Fig. 1. The PXD consists of DEPFET pixel sensors, 60  
 22 and its innermost radius is 1.4 cm from the beam interaction 61  
 23 point (IP). A detailed description of the SVD appears in Sec. 2.

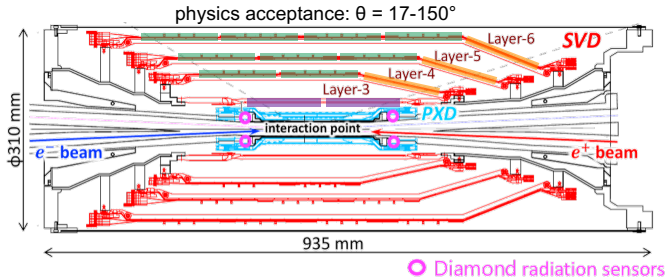


Figure 1: Schematic cross-sectional view of the VXD. The SVD is red, the PXD is light blue, and the IP beam pipe diamonds are pink circles. In the upper half of the VXD the locations of the three types of SVD DSSDs are indicated by boxes in three colors: purple for small sensors, green for large sensors, and orange for trapezoidal sensors as described in Tab. 1.

24 Diamond sensors [3], used to monitor the radiation dose and 66  
 25 for the beam abort system, are mounted on the IP beam pipe and 67  
 26 the bellows pipes outside of the VXD. The pink circles in Fig. 1 68  
 27 indicate the locations of the diamond sensors on the IP beam 69  
 28 pipe. The diamond’s measured doses are used to estimate the 70  
 29 dose in the SVD. The diamond system also sends beam abort 71  
 30 requests to SuperKEKB if the radiation level gets too high to 72  
 31 avoid severe damage to the detector.

## 32 2. Belle II Silicon Vertex Detector

33 The SVD is crucial for extrapolating the tracks to the PXD 77  
 34 to measure the decay vertices with the PXD and point at a 78  
 35 region-of-interest limiting the PXD readout data volume. Other 79  
 36 roles of the SVD are the standalone track reconstruction of low- 80  
 37 momentum charged particles and their particle identification using 81  
 38 ionization energy deposits. The SVD also plays a critical 82  
 39 role in the decay vertex measurement in the case of long-lived 83  
 40 particles like  $K_S$  mesons, which decay inside the SVD volume. 84

41 The SVD [4] consists of four layers of double-sided silicon 85  
 42 strip detectors (DSSDs). The material budget of the SVD is 86  
 43 about 0.7% of a radiation length per layer. On each DSSD 87  
 44 plane, a local coordinate is defined with  $u$  and  $v$ :  $u$ -axis along 88  
 45  $n$ -side strips and  $v$ -axis perpendicular to  $u$ -axis. In other words, 89  
 46  $p$ -side strips and  $n$ -side strips provide  $u$  and  $v$  information, re- 90  
 47 spectively. In the cylindrical coordinate,  $u$  corresponds to  $r-\varphi$  91  
 48 information and  $v$  corresponds to  $z$  information. The SVD consists 92  
 49 of three types of sensors: “small” rectangular sensors in 93  
 50 layer 3, “large” rectangular sensors in the barrel region of lay- 94  
 51 ers 4, 5, and 6, and “trapezoidal” sensors in the forward region 95  
 52 of layers 4, 5, and 6, which is slanted. They are indicated by 96  
 53 purple, green, and orange boxes in Fig. 1. The main character- 97  
 54 istics of these three types of sensors are summarized in Tab. 1. 98

The sensors are manufactured by two companies: the small and large sensors by Hamamatsu and trapezoidal sensors by Micron. The full depletion voltage is 60 V for Hamamatsu sensors and 20 V for Micron sensors; both types of sensors are operated at 100 V. In total, 172 sensors are assembled, corresponding to a sensor area of 1.2 m<sup>2</sup> and approximately 224,000 readout strips.

	Small	Large	Trapezoidal
No. of u/p-strips	768	768	768
u/p-strip pitch	50 $\mu\text{m}$	75 $\mu\text{m}$	50–75 $\mu\text{m}$
No. of v/n-strips	768	512	512
v/n-strip pitch	160 $\mu\text{m}$	240 $\mu\text{m}$	240 $\mu\text{m}$
Thickness	320 $\mu\text{m}$	320 $\mu\text{m}$	300 $\mu\text{m}$
Manufacturer	Hamamatsu		Micron

Table 1: Table of the main characteristics of the three types of sensors. Only readout strips are taken into account for number of strips and strip pitch. All sensors have one intermediate floating strip between two readout strips.

Sensor strips are AC coupled to the front-end ASIC, the APV25 [5], which was originally developed for the CMS Silicon Tracker. The APV25 tolerates more than 100 Mrad of radiation. It has 128 channels with a shaping time of about 50 ns. For the SVD, the APV25 is operated in “multi-peak” mode. The mechanism of the data sampling in the multi-peak mode is explained in Fig. 2. The chip samples the height of the signal waveform with the 32 MHz clock (31 ns period) and stores each sample’s information in an analog ring buffer. Since the bunch-crossing frequency is eight times faster than the sampling clock, the stored samples are not synchronous to the beam collision, in contrast to CMS, which motivates operation in the multi-peak mode. In the present readout configuration (the six-samples mode), at every reception of the Belle II global Level-1 trigger, the chip reads out six successive samples of the signal waveform stored in the buffers. The six-samples mode offers a wide enough time window ( $6 \times 31 \text{ ns} = 187 \text{ ns}$ ) to accommodate large timing shifts of the trigger. In preparation for operation with higher luminosity, where background occupancy, trigger dead-time, and the data size increase, we developed the three/six-mixed acquisition mode (mixed-mode). The mixed-mode is a new method to read out the signal samples from the APV25, in which the number of the samples changes between three and six in each event, depending on the timing precision of each Level-1 trigger signal in that event. For triggers with precise timing, three-samples data are read out and the data have half time window and half data size compared to ones of six-samples data, resulting in the reduction of the effects due to higher luminosity. This functionality was already implemented in the running system and confirmed by a few hours of smooth physics data taking. Before we start to use the mixed-mode, the effect on the performance due to the change of the acquisition mode is to be assessed. As the first step, the effect in the hit efficiency was evaluated as described in Sec. 3.

The APV25 chips are mounted on each middle sensor (chip-on-sensor concept) with thermal isolation foam in between. The merit of this concept is shorter signal propagation length, leading to smaller capacitance of the signal line and hence reduced

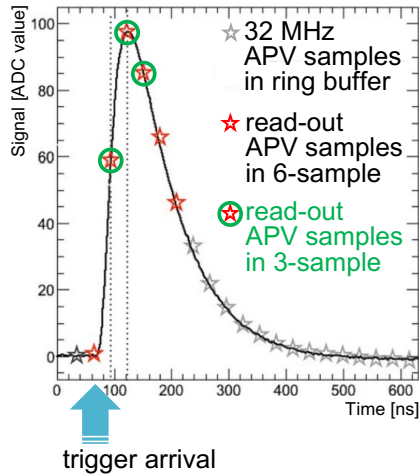


Figure 2: Example of sampling in “multi-peak” mode of the APV25. The black line shows the signal waveform after the CR-RC shaper circuit. The stars show the sampled signal height recorded in the analog ring buffer according to the 32 MHz sampling clock. The red stars indicate the six successive samples read out at the trigger reception in the six-samples mode. The red stars with a green circle indicate the samples read out in the three-samples acquisition.

99 noise level. To minimize the material budget the APV25 chips  
 100 on the sensor are thinned down to 100  $\mu\text{m}$ . The APV25 chips  
 101 are mounted on a single side of the sensor and readout of the  
 102 signals from the opposite side is performed via wrapped flexible  
 103 printed circuits. The power consumption of the APV25  
 104 chip is 0.4 W/chip and 700 W in the entire SVD. The chips are  
 105 cooled by a bi-phase  $-20^\circ\text{C}$   $\text{CO}_2$  evaporative cooling system.

### 3. Performance

107 Since March 2019, the SVD has been operating reliably and  
 108 smoothly for two and a half years. The total fraction of masked  
 109 strips is about 1%. There was only one issue where one APV25  
 110 chip (out of 1,748 chips) was disabled during the spring of  
 111 2019, which was remediated by reconnecting a cable in the  
 112 summer of 2019.

113 The SVD has also demonstrated stable and excellent perfor-  
 114 mance [6]. The hit efficiency is continuously over 99% in most  
 115 of the sensors. The cluster charge distributions are also reason-  
 116 able. On the u/p-side, the most probable values agree with the  
 117 calculated charge amount induced by MIPs within the uncer-  
 118 tainty in calibration. On the v/n-side, 10–30% of the collected  
 119 charge is lost compared to the signal collected on the u/p-side,  
 120 due to the presence of the floating strip combined with the large  
 121 pitch on the v/n-side. The most probable values of the cluster  
 122 signal-to-noise ratio distributions range from 13 to 30.

123 We measured the cluster position resolution by analyzing the  
 124  $e^+e^- \rightarrow \mu^+\mu^-$  data [7]. The resolution is estimated from the  
 125 residual between the cluster position and the track position, not  
 126 biased by the target cluster, after subtracting the effect of the  
 127 track extrapolation error. The cluster position resolutions for  
 128 different incident angles are shown in Fig. 3. The observed  
 129 resolution has the expected shape, showing a minimum at the  
 130 incident angle for which the projection of the track along the

131 direction perpendicular to the strips on the detector plane cor-  
 132 responds to two strip pitches. Given the various sensor pitches  
 133 with one floating strip, the minimum is expected at 14 (21) de-  
 134 grees on the v/n-side and at 4 (7) degrees on the u/p-side, re-  
 135 spectively for layer 3 (4, 5, and 6). The resolution for normal  
 136 incident angle is also in good agreement with the expected dig-  
 137 ital resolution, that is 23 (35)  $\mu\text{m}$  on the v/n-side, 7 (11)  $\mu\text{m}$   
 138 on the u/p-side, respectively for layer 3 (4, 5, and 6). Still, some  
 139 studies are ongoing to improve the resolution especially for the  
 140 layer-3 u/p-side, where at normal incidence a slightly higher  
 141 resolution is measured (9  $\mu\text{m}$ ) compared to the expectations.

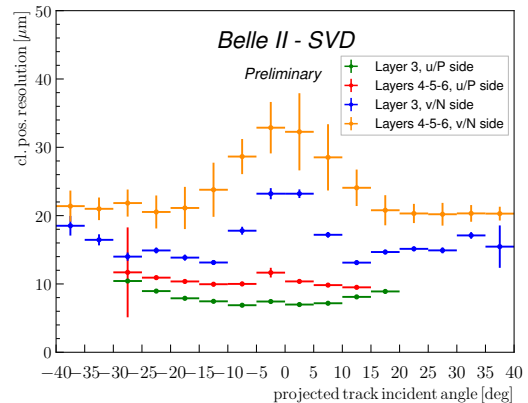


Figure 3: The SVD cluster position resolution depending on the projected track incident angle. The green (blue) plot shows the resolution in the u/p-side (n/v-side) of layer-3 sensors, and the red (yellow) one shows the u/p-side (n/v-side) of layers-4, 5, and 6 sensors.

142 The cluster hit-time resolution was also evaluated in candi-  
 143 date hadronic events<sup>1</sup> using the reference event time estimated  
 144 by the Central Drift Chamber (CDC) outside of the SVD. The  
 error on the event time, about 0.7 ns, was subtracted to evalu-  
 145 ate the intrinsic SVD hit-time resolution. The resulting resolu-  
 146 tion is 2.9 ns on the u/p-side and 2.4 ns on the v/n-side. With  
 147 such precise hit-time information, it is possible to reject off-  
 148 time background hits efficiently. The hit-time distributions for  
 149 signal<sup>2</sup> and background<sup>3</sup> are shown in Fig. 4. The signal dis-  
 150 tribution has a narrow peak, while the background hit-time dis-  
 151 tribution is broad and almost flat in the signal peak region. The  
 152 separation power of the hit-time is high, as expected. For ex-  
 153 ample, if we reject hits with the hit-time less than  $-38$  ns in this  
 154 plot, we can reject 45% of the background hits while keeping  
 155 99% of the signal hits. The background rejection based on the  
 156 hit-time is essential to sustain the good tracking performance in  
 157 the future high beam background condition.

158 The performance in three-samples data was compared with  
 159 that in six-samples data to evaluate the performance in the  
 160 mixed-mode. If the trigger timing has no deviation, the three-  
 161 samples data will show comparable performance to the six-  
 162 samples data because the relevant part of the signal wave-  
 163 form to evaluate the necessary signal properties, i.e., the signal

<sup>1</sup>The events with more than three good tracks and not like Bhabha scattering.

<sup>2</sup>The clusters found to be used in the tracks in the hadronic events.

<sup>3</sup>The clusters in events triggered by delayed-Bhabha pseudo-random trigger.

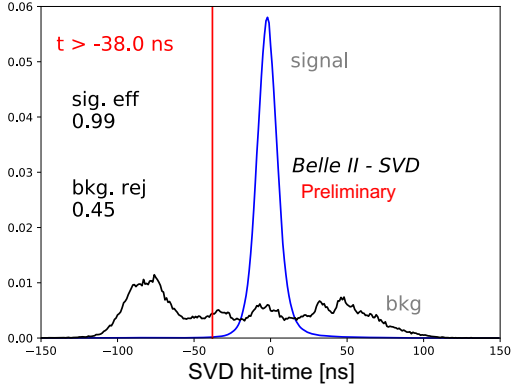


Figure 4: Example of the background hit rejection using hit-time. The blue distribution shows the signal, and the black distribution shows the background. Assuming the hit-time cut at  $-38$  ns, the signal hit efficiency of 99% and the background hit rejection of 45% are achieved.

height and the signal timing can be accommodated in the three-sample's time window. However, when the trigger has a jitter and the timing shift happens, some part of the signal waveform can be out of the three-sample's time window, and the reconstruction performance deteriorates. We examined the effect on the hit efficiency as a function of the trigger timing shift. The effect is evaluated by the relative hit efficiency, which is defined as the ratio of the hit efficiency in the three-samples data to the one in the six-samples data. For this study, the three-samples data are emulated in the offline analysis from the six-samples data by selecting consecutive three samples at a fixed latency with respect to the Level-1 trigger signal. The trigger timing shift is evaluated by the CDC event time. The resulting relative efficiencies as a function of the trigger timing shift in the hadronic events are shown in Fig. 5. The decreasing trend is observed for the shift of the trigger timing, as expected. As a result, the relative efficiency is over 99.9% for the trigger timing shift within  $\pm 30$  ns, which is almost all the events.

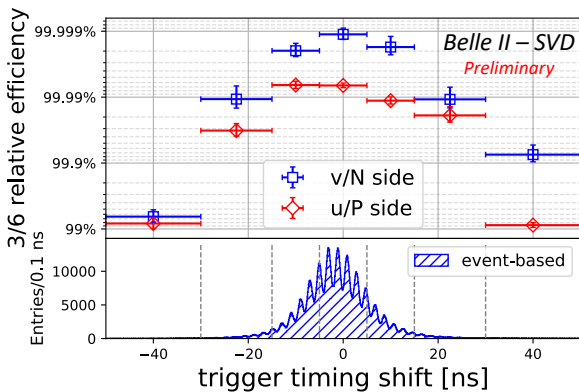


Figure 5: The relative hit efficiencies (the ratios of the hit efficiency in the three-samples data to the one in the six-samples data) as a function of the trigger timing shift for v/n-side (blue square) and u/p-side (red diamond). The positive (negative) trigger timing shift corresponds to early (late) trigger timing.

#### 4. Beam-related background effects on SVD

The beam-related background (BG) increases the hit occupancy of the SVD, which in turn degrades the tracking performance. Considering this performance degradation, we set the occupancy limit in layer-3 sensors to be about 3%, which will be loosened roughly by a factor of two after we apply the hit-time rejection described in Sec. 3. With the current luminosity, the average hit occupancy in layer-3 sensors is below 0.5%. However, the projection of the hit occupancy at the luminosity of  $8 \times 10^{35} \text{ cm}^{-2}\text{s}^{-1}$  is about 3% in layer-3 sensors. The projected occupancy comes from the Monte Carlo (MC) simulation scaled by the data/MC ratio determined from the BG data of the current beam optics. The corresponding integrated dose, using the data/MC-rescaled BG extrapolation, is about 0.2 Mrad/smy, and the equivalent 1-MeV neutron fluence is about  $5 \times 10^{11} \text{ n}_{\text{eq}}/\text{cm}^2/\text{smy}$  (smy: Snowmass Year =  $10^7$  sec). Considering the radiation hardness of the SVD sensors, about 10 Mrad and about  $10^{13} \text{ n}_{\text{eq}}/\text{cm}^2$ , based on the experience of similar DSSD sensors used in the BaBar Silicon Vertex Tracker [8], we expect to be able to safely operate the SVD even for ten years at high luminosity, with safety margin of factor two to three against BG extrapolation. The long-term BG extrapolation is affected by large uncertainties from the optimization of collimator settings in MC and the future evolution of the beam injection background, which is not simulated. This uncertainty, together with the relatively small safety factor of two to three between the BG extrapolation and the detector limits, motivates the VXD upgrade to improve the tolerance of the hit rates and the radiation damage, and the technology assessment is ongoing for multiple sensor options.

In the first two and a half years of operation, the integrated dose in the layer-3 mid-plane sensors, which are the most exposed in the SVD, is estimated to be 70 krad. The estimation is based on the measured dose by the diamonds on the beam pipe exploiting the measured correlation between the SVD occupancy and the diamond dose [9]. Thanks to a new random trigger line recently introduced, we improved the dose analysis, removing an overestimation of about factor three in the previous study. The new estimate still has an uncertainty of about 50% mainly due to the unavailability of this newly introduced trigger before December 2020. Assuming the dose/ $\text{n}_{\text{eq}}$  fluence ratio of  $2.3 \times 10^9 \text{ n}_{\text{eq}}/\text{cm}^2/\text{krad}$  from MC, 1-MeV equivalent neutron fluence is evaluated to be about  $1.6 \times 10^{11} \text{ n}_{\text{eq}}/\text{cm}^2$ .

The effect of the integrated dose on the sensor leakage current is measured, and the results show a clear linear correlation as in the upper plot of Fig. 6. The slopes for all the sensors are  $2\text{--}5 \text{ }\mu\text{A}/\text{cm}^2/\text{Mrad}$ , as summarized in the lower plot of Fig. 6. The large variations can be explained by temperature effects and the deviation of sensor-by-sensor dose from the average in each layer used in the estimation. The slopes are in the same order of magnitude as previously measured in the BaBar experiment [8],  $1 \text{ }\mu\text{A}/\text{cm}^2/\text{Mrad}$  at  $20^\circ\text{C}$ . The precise temperature in layer 3 of the SVD is unknown but expected to be in a similar regime. While the leakage current is increasing, the impact on the strip noise is suppressed by the short shaping time (50 ns) in APV25. It is expected to be comparable to the strip-capacitive

239 noise only after 10 Mrad irradiation and not problematic for ten  
 240 years where the integrated dose is estimated to be 2 Mrad.

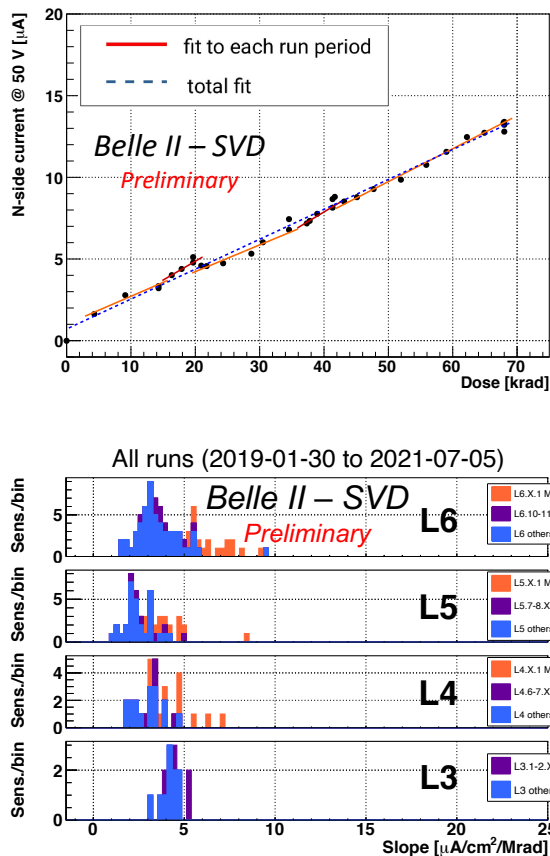


Figure 6: (upper) Effect of the integrated dose on the leakage current in the n/v-  
 side of one layer-3 sensor. The slope is fitted for each run period (solid red line)  
 and all the runs (dashed blue line). Both fit results agree with each other and are  
 consistent with the linear increase. (lower) The fit results of all the sensors for  
 all runs. The sensors are classified as trapezoidal sensors in the forward region  
 (Micron), sensors around the midplane, and the others.

241 The evolution of the noise with the integrated dose is shown  
 242 in Fig. 7. The noise increase of 20–25% is observed in layer  
 243 3, but this does not affect the SVD performance. This noise  
 244 increase is likely due to the radiation effects on the sensor sur-  
 245 face. Fixed oxide charges on sensor surface increase with dose,  
 246 with some saturation expected at around 100 krad, enlarging  
 247 also non-linearly the inter-strip capacitance, also expected to  
 248 saturate with dose. The noise saturation is already observed on  
 249 the v/n-side and also starts to be seen on the u/p-side.  
 250 The full depletion voltage of the sensor is also a key property  
 251 that can be affected by the radiation damage. It can be measured  
 252 from the v/n-side strip noise, which suddenly decreases at the  
 253 full depletion voltage because the sensor substrate is n-type and  
 254 thus the v/n-side strips are only fully isolated at full depletion.  
 255 From this measurement full depletion voltages consistent with  
 256 measurements performed on the bare sensors before the instal-  
 257 lation were obtained, ranging from 20 to 60 V, and so far no  
 258 change in full depletion voltage is observed in the first two and  
 259 a half years of operation, which is consistent with the expecta-  
 260 tion from low integrated neutron fluence of  $1.6 \times 10^{11} \text{ n}_{\text{eq}}/\text{cm}^2$ .

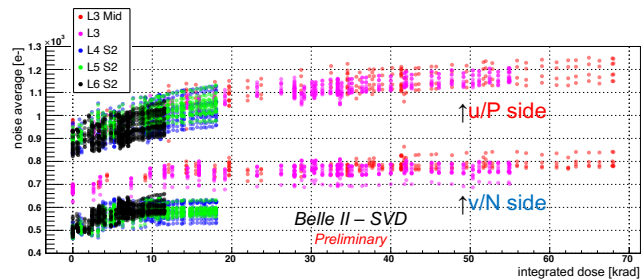


Figure 7: Effect of the integrated dose on the noise average in electron. The  
 upper (lower) series shows the u/p-side (v/n-side) results, respectively.

## 261 5. Conclusions

262 The SVD has been taking data in Belle II since March 2019  
 263 smoothly and reliably. The detector performance is excellent  
 264 and agrees with expectations. We are ready to cope with the  
 265 increased background during higher luminosity running by re-  
 266 jecting the off-time background hits using hit-time and operat-  
 267 ing in the three/six-mixed acquisition mode. In the recent study,  
 268 the efficiency loss in the three-samples data is confirmed to be  
 269 less than 0.1% for the trigger timing shift within  $\pm 30$  ns. The  
 270 observed first effects of radiation damage are also within expecta-  
 271 tion and do not affect the detector performance.

## 272 Acknowledgments

273 This project has received funding from the European Union's  
 274 Horizon 2020 research and innovation programme under the  
 275 Marie Skłodowska-Curie grant agreements No 644294 and  
 822070. This work is supported by MEXT, WPI, and  
 JSPS (Japan); ARC (Australia); BMBWF (Austria); MSMT  
 (Czechia); CNRS/IN2P3 (France); AIDA-2020 (Germany);  
 DAE and DST (India); INFN (Italy); NRF and RSRI (Korea);  
 and MNiSW (Poland).

## 276 References

- [1] T. Abe, et al., Belle II Technical Design Report (2010). arXiv:1011.0352.
- [2] Y. Ohnishi, et al., Accelerator design at SuperKEKB, Prog. Theor. Exp. Phys. 2013 (3), 03A011 (03 2013).
- [3] S. Bacher, et al., Performance of the diamond-based beam-loss monitor system of Belle II, Nucl. Instrum. Methods Phys. Res., Sect. A 997 (2021) 165157. arXiv:2102.04800.
- [4] K. Adamczyk, et al., The Belle II silicon vertex detector assembly and mechanics, Nucl. Instrum. Methods Phys. Res., Sect. A 845 (2017) 38–42, proceedings of the Vienna Conference on Instrumentation 2016.
- [5] M. J. French, et al., Design and results from the APV25, a deep sub-micron CMOS front-end chip for the CMS tracker, Nucl. Instrum. Methods Phys. Res., Sect. A 466 (2001) 359–365.
- [6] G. Rizzo, et al., The Belle II Silicon Vertex Detector: Performance and Operational Experience in the First Year of Data Taking, JPS Conf. Proc. 34 (2021) 010003.
- [7] R. Leboucher, et al., Measurement of the cluster position resolution of the Belle II Silicon Vertex Detector, these NIMA Conference Proceedings.
- [8] B. Aubert, et al., The BaBar detector: Upgrades, operation and performance, Nucl. Instrum. Methods Phys. Res., Sect. A 729 (2013) 615–701.
- [9] L. Massaccesi, Performance study of the SVD detector of Belle II and future upgrades, master thesis, Dipartimento di Fisica E. Fermi, Università di Pisa (2021).  
 URL <https://docs.belle2.org/record/2759/>